

World Journal of *Stem Cells*

World J Stem Cells 2023 November 26; 15(11): 989-1034



MINIREVIEWS

- 989 How to enhance the ability of mesenchymal stem cells to alleviate intervertebral disc degeneration
Zhang QX, Cui M

ORIGINAL ARTICLE**Basic Study**

- 999 Hypoxia and inflammatory factor preconditioning enhances the immunosuppressive properties of human umbilical cord mesenchymal stem cells
Li H, Ji XQ, Zhang SM, Bi RH
- 1017 Dissecting molecular mechanisms underlying ferroptosis in human umbilical cord mesenchymal stem cells: Role of cystathionine γ -lyase/hydrogen sulfide pathway
Hu B, Zhang XX, Zhang T, Yu WC

ABOUT COVER

Editorial Board Member of *World Journal of Stem Cells*, Jyoti Anand Kode, MSc, PhD, Associate Professor, Senior Scientist, Principal Investigator, Kode Lab, Tumor Immunology and Immunotherapy Group, Facility for Immunomodulatory Activity Testing, Anti-Cancer Drug Screening Facility, Advanced Centre for Treatment, Research and Education in Cancer, Tata Memorial Centre, Homi Bhabha National Institute, Navi Mumbai 410210, Maharashtra, India. jkode@actrec.gov.in

AIMS AND SCOPE

The primary aim of *World Journal of Stem Cells (WJSC, World J Stem Cells)* is to provide scholars and readers from various fields of stem cells with a platform to publish high-quality basic and clinical research articles and communicate their research findings online. *WJSC* publishes articles reporting research results obtained in the field of stem cell biology and regenerative medicine, related to the wide range of stem cells including embryonic stem cells, germline stem cells, tissue-specific stem cells, adult stem cells, mesenchymal stromal cells, induced pluripotent stem cells, embryonal carcinoma stem cells, hemangioblasts, lymphoid progenitor cells, etc.

INDEXING/ABSTRACTING

The *WJSC* is now abstracted and indexed in Science Citation Index Expanded (SCIE, also known as SciSearch®), Journal Citation Reports/Science Edition, PubMed, PubMed Central, Scopus, Biological Abstracts, BIOSIS Previews, Reference Citation Analysis, China National Knowledge Infrastructure, China Science and Technology Journal Database, and Superstar Journals Database. The 2023 Edition of Journal Citation Reports® cites the 2022 impact factor (IF) for *WJSC* as 4.1; IF without journal self cites: 3.9; 5-year IF: 4.5; Journal Citation Indicator: 0.53; Ranking: 15 among 29 journals in cell and tissue engineering; Quartile category: Q3; Ranking: 99 among 191 journals in cell biology; and Quartile category: Q3. The *WJSC*'s CiteScore for 2022 is 8.0 and Scopus CiteScore rank 2022: Histology is 9/57; Genetics is 68/325; Genetics (clinical) is 19/90; Molecular Biology is 119/380; Cell Biology is 95/274.

RESPONSIBLE EDITORS FOR THIS ISSUE

Production Editor: *Xiang-Di Zhang*; Production Department Director: *Xu Guo*; Editorial Office Director: *Jia-Ru Fan*.

NAME OF JOURNAL

World Journal of Stem Cells

ISSN

ISSN 1948-0210 (online)

LAUNCH DATE

December 31, 2009

FREQUENCY

Monthly

EDITORS-IN-CHIEF

Shengwen Calvin Li, Carlo Ventura

EDITORIAL BOARD MEMBERS

<https://www.wjgnet.com/1948-0210/editorialboard.htm>

PUBLICATION DATE

November 26, 2023

COPYRIGHT

© 2023 Baishideng Publishing Group Inc

INSTRUCTIONS TO AUTHORS

<https://www.wjgnet.com/bpg/gerinfo/204>

GUIDELINES FOR ETHICS DOCUMENTS

<https://www.wjgnet.com/bpg/GerInfo/287>

GUIDELINES FOR NON-NATIVE SPEAKERS OF ENGLISH

<https://www.wjgnet.com/bpg/gerinfo/240>

PUBLICATION ETHICS

<https://www.wjgnet.com/bpg/GerInfo/288>

PUBLICATION MISCONDUCT

<https://www.wjgnet.com/bpg/gerinfo/208>

ARTICLE PROCESSING CHARGE

<https://www.wjgnet.com/bpg/gerinfo/242>

STEPS FOR SUBMITTING MANUSCRIPTS

<https://www.wjgnet.com/bpg/GerInfo/239>

ONLINE SUBMISSION

<https://www.f6publishing.com>

Basic Study

Dissecting molecular mechanisms underlying ferroptosis in human umbilical cord mesenchymal stem cells: Role of cystathionine γ -lyase/hydrogen sulfide pathway

Bin Hu, Xiang-Xi Zhang, Tao Zhang, Wan-Cheng Yu

Specialty type: Cell and tissue engineering**Provenance and peer review:**

Unsolicited article; Externally peer reviewed.

Peer-review model: Single blind**Peer-review report's scientific quality classification**Grade A (Excellent): 0
Grade B (Very good): B
Grade C (Good): C, C
Grade D (Fair): D
Grade E (Poor): 0**P-Reviewer:** Jaing TH, Taiwan; Ventura C, Italy; Wang Q, China; Li SC, United States**Received:** September 2, 2023**Peer-review started:** September 2, 2023**First decision:** October 19, 2023**Revised:** October 25, 2023**Accepted:** November 17, 2023**Article in press:** November 17, 2023**Published online:** November 26, 2023**Bin Hu, Xiang-Xi Zhang, Tao Zhang, Wan-Cheng Yu**, Department of Cardiovascular Surgery, Shandong Provincial Hospital Affiliated to Shandong First Medical University, Jinan 250062, Shandong Province, China**Corresponding author:** Wan-Cheng Yu, Doctor, MD, Postdoc, Surgeon, Department of Cardiovascular Surgery, Shandong Provincial Hospital Affiliated to Shandong First Medical University, No. 324 Jingwu Weiqi Road, Jinan 250062, Shandong Province, China. yuwancheng123@126.com

Abstract

BACKGROUND

Ferroptosis can induce low retention and engraftment after mesenchymal stem cell (MSC) delivery, which is considered a major challenge to the effectiveness of MSC-based pulmonary arterial hypertension (PAH) therapy. Interestingly, the cystathionine γ -lyase (CSE)/hydrogen sulfide (H_2S) pathway may contribute to mediating ferroptosis. However, the influence of the CSE/ H_2S pathway on ferroptosis in human umbilical cord MSCs (HUCMSCs) remains unclear.

AIM

To clarify whether the effect of HUCMSCs on vascular remodelling in PAH mice is affected by CSE/ H_2S pathway-mediated ferroptosis, and to investigate the functions of the CSE/ H_2S pathway in ferroptosis in HUCMSCs and the underlying mechanisms.

METHODS

Erastin and ferrostatin-1 (Fer-1) were used to induce and inhibit ferroptosis, respectively. HUCMSCs were transfected with a vector to overexpress or inhibit expression of CSE. A PAH mouse model was established using 4-wk-old male BALB/c nude mice under hypoxic conditions, and pulmonary pressure and vascular remodelling were measured. The survival of HUCMSCs after delivery was observed by *in vivo* bioluminescence imaging. Cell viability, iron accumulation, reactive oxygen species production, cystine uptake, and lipid peroxidation in HUCMSCs were tested. Ferroptosis-related proteins and S-sulphydrated Kelch-like ECH-associating protein 1 (Keap1) were detected by western blot analysis.

RESULTS

In vivo, CSE overexpression improved cell survival after erastin-treated HUCMSC delivery in mice with hypoxia-induced PAH. *In vitro*, CSE overexpression improved H₂S production and ferroptosis-related indexes, such as cell viability, iron level, reactive oxygen species production, cystine uptake, lipid peroxidation, mitochondrial membrane density, and ferroptosis-related protein expression, in erastin-treated HUCMSCs. In contrast, *in vivo*, CSE inhibition decreased cell survival after Fer-1-treated HUCMSC delivery and aggravated vascular remodelling in PAH mice. *In vitro*, CSE inhibition decreased H₂S levels and restored ferroptosis in Fer-1-treated HUCMSCs. Interestingly, upregulation of the CSE/H₂S pathway induced Keap1 S-sulfhydration, which contributed to the inhibition of ferroptosis.

CONCLUSION

Regulation of the CSE/H₂S pathway in HUCMSCs contributes to the inhibition of ferroptosis and improves the suppressive effect on vascular remodelling in mice with hypoxia-induced PAH. Moreover, the protective effect of the CSE/H₂S pathway against ferroptosis in HUCMSCs is mediated *via* S-sulfhydrated Keap1/nuclear factor erythroid 2-related factor 2 signalling. The present study may provide a novel therapeutic avenue for improving the protective capacity of transplanted MSCs in PAH.

Key Words: Human umbilical cord mesenchymal stem cells; Cystathionine γ -lyase/hydrogen sulfide pathway; Ferroptosis; Pulmonary arterial hypertension; S-sulfhydration

©The Author(s) 2023. Published by Baishideng Publishing Group Inc. All rights reserved.

Core Tip: Regulation of the cystathionine γ -lyase (CSE)/hydrogen sulfide (H₂S) pathway in human umbilical cord mesenchymal stem cells (HUCMSCs) contributes to the inhibition of ferroptosis and improves the suppressive effect of HUCMSCs on vascular remodelling in hypoxia-induced pulmonary arterial hypertension (PAH) mice. Moreover, the protective effect of the CSE/H₂S pathway against ferroptosis in HUCMSCs was mediated *via* S-sulfhydrated Kelch-like ECH-associating protein 1/nuclear factor erythroid 2-related factor 2 signalling. The present study may provide a novel therapeutic avenue for improving the protective capacity of transplanted MSCs in PAH.

Citation: Hu B, Zhang XX, Zhang T, Yu WC. Dissecting molecular mechanisms underlying ferroptosis in human umbilical cord mesenchymal stem cells: Role of cystathionine γ -lyase/hydrogen sulfide pathway. *World J Stem Cells* 2023; 15(11): 1017-1034

URL: <https://www.wjgnet.com/1948-0210/full/v15/i11/1017.htm>

DOI: <https://dx.doi.org/10.4252/wjsc.v15.i11.1017>

INTRODUCTION

Mesenchymal stem cells (MSCs), derived from placenta, bone marrow, adipose, or other tissues, have emerged as a new regenerative therapy for pulmonary arterial hypertension (PAH) over the last decade[1]. MSC delivery significantly inhibits pulmonary artery remodelling, resulting in the reduced progression of PAH. However, low cell retention and engraftment after cell delivery are considered major challenges to the effectiveness of MSC-based therapy[2]. Interestingly, increasing evidence indicates that programmed cell death (PCD) is closely linked to the low engraftment and survival rates of transplanted MSCs[3].

Ferroptosis is a novel type of PCD with distinct properties. Ferroptosis essentially consists of polyunsaturated fatty acid-containing phospholipid synthesis and peroxidation, iron metabolism, and mitochondrial metabolism, which result in oxidative stress and lipid peroxidation, triggering cell death[4]. Studies have shown a relationship between ferroptosis and MSCs; ferroptosis can be induced by erastin in MSCs[5,6]. Inhibiting ferroptosis maintained the viability and differentiation of MSCs[7,8]. Moreover, suppressing ferroptosis worsened MSC fate and enhanced the exposure and efficacy of transplanted MSCs in live disease[9]. However, few studies have directly evaluated the effect of ferroptosis on MSC delivery in PAH.

Decreased antioxidative stress can cause ferroptosis[10]. In addition, the mediation of antioxidative stress-related proteins, such as nuclear factor erythroid 2-related factor 2 (Nrf2), can inhibit ferroptosis[11]. Thus, understanding the signalling pathways that maintain redox balance will provide new approaches for inhibiting ferroptosis. The novel gaseous mediator hydrogen sulfide (H₂S) has been shown to exert protective effects, including its antioxidant properties [12]. Therefore, the impact of H₂S on the contribution of antioxidative stress to decreased ferroptosis is worth exploring. In mammalian cells, cystathionine γ -lyase (CSE) is predominantly responsible for endogenous H₂S production in the cardiovascular system[13]. However, the effect of CSE on the ferroptosis of MSCs remains unclear.

Hence, the present study aimed to clarify whether ferroptosis is involved in the therapeutic effect of human umbilical cord MSCs (HUCMSCs) in PAH mice. Furthermore, we investigated the role of the CSE/H₂S pathway in ferroptosis in HUCMSCs.

MATERIALS AND METHODS

Cell culture

Primary HUCMSCs were purchased from ScienCell Research Laboratories, Inc. HUCMSCs were cultured in MSC medium (7501, ScienCell Research Laboratories, United States) containing 5% foetal bovine serum, 1% penicillin/streptomycin, and 1% MSC growth supplement at 37 °C in a 5% CO₂ atmosphere. HUCMSCs at passages three to five were used in this study.

Cell transfection

HUCMSCs were transduced with a lentiviral vector expressing firefly luciferase (HBLV-LUC-BSD, Hanbio, China) in serum-free medium containing 3 µg/mL blasticidin (SBR00022, Sigma-Aldrich, United States) at a multiplicity of infection of 100. Transduction was analysed by luciferase imaging 72 h after transfection. The expression of LUC was confirmed by measuring luciferase activity [*in vivo* imaging system (IVIS) Lumina imaging station, Caliper Life Sciences]. Surface markers and the differentiation of HUCMSCs-LUC into osteoblasts and adipocytes were evaluated as previously described[14]. The antibodies that were used are shown in [Supplementary Table 1](#).

Short hairpin RNAs targeting CSE were designed, cloned, and inserted into a modified pLKO.1-TRC vector by GenePharma Co. Ltd. (Shanghai, CHN). To genetically engineer cells to overexpress CSE, the open reading frame of human CSE was cloned and inserted into the vector pLVX-IRES-Puro by GenePharma Co. Ltd. (Shanghai, CHN). HUCMSCs-LUC were transfected with the pLKO.1-sh-CSE vector (HUCMSC/sh-CSE), negative control vector (HUCMSCs/sh-NC), PLVX-CSE-Puro vector (HUCMSCs/CSE), or PLVX-empty-Puro vector (HUCMSCs/NC) using Lipofectamine 2000 (11668019, Invitrogen, United States). After 48 h, the transfection efficacy was determined using western blot and real-time polymerase chain reaction (RT-PCR) ([Supplementary Figure 1](#)).

Drug treatments

Erastin (S7242), ferrostatin-1 (Fer-1, S7243), and the Nrf2 inhibitor brusatol (S7956, 10 nM, 6 h) were purchased from Selleck Chemicals (Houston, United States) and initially dissolved in DMSO before being diluted in the culture medium to their final concentration.

Quantification of cell viability

Cell Counting Kit-8 (CCK8, 96992, Sigma-Aldrich, United States) was used to examine cell viability according to the manufacturer's instructions. Briefly, cells were seeded at a density of 5000 cells/well in 96-well plates in three replicates and incubated overnight. At the end of the different treatments, CCK8 reagent was added to each well and incubated for 2 h. The optical density (OD) values at 450 nm were measured using a plate reader (Bio-Rad).

Lactase dehydrogenase release assay

Lactate dehydrogenase (LDH) release was measured using an LDH cytotoxicity detection kit (CK12, Dojindo Laboratory, JPN) in accordance with the manufacturer's instructions to evaluate cell membrane integrity. In brief, cells were seeded at a density of 5000 cells/well in 96-well plates. At the end of the different treatments, 100 µL of fresh reaction mixture was added to each well and incubated for 30 min, and the OD values at 490 nm were measured using a microplate reader.

Animal experiments

Animal procedures were performed in compliance with the Institutional Animal Care and Use Committee of Wuhan Servicebio Technology Co., Ltd., China (No. 2022231). Four-week-old male mice (BALB/c nude mice) were used to establish a hypoxia-induced PAH mouse model. The mice were obtained from Wuhan Servicebio Technology Co., Ltd. (Wuhan, China) and cared for in strict accordance with the Guidelines for the Care and Use of Laboratory Animals of the National Institutes of Health. All animals were housed in the same specific pathogen-free room under a constant temperature and humidity on a 12-h light and 12-h dark cycle, and the animals were fed sterile food and water *ad libitum*. Each animal was considered one experimental unit. Researchers who analysed the data were blinded to the group allocation until all the statistical results were finally obtained.

The mice (totally 42) were numbered and divided into the following seven groups based on a table of random numbers: Control group: The mice received phosphate buffered saline (PBS) ($n = 6$); hypoxia group: The mice were exposed to hypoxia under 10% O₂ for 4 wk ($n = 6$); HUCMSCs group: After 2 wk of exposure to hypoxia, the mice were injected with 1.5×10^5 HUCMSCs-LUC per mouse *via* the tail vein and then housed under hypoxia for 2 wk ($n = 6$); HUCMSCs + erastin group: After 2 wk of exposure to hypoxia, the mice were infected with 1.5×10^5 HUCMSCs-LUC that were treated with erastin (4 µM, 6 h) per mouse *via* the tail vein and then housed under hypoxia for 2 wk ($n = 6$); HUCMSCs/CSE + erastin group: After 2 wk of exposure to hypoxia, the mice were injected with 1.5×10^5 HUCMSCs-LUC/CSE that were treated with erastin (4 µM, 6 h) per mouse *via* the tail vein and then housed under hypoxia for 2 wk ($n = 6$); HUCMSCs + Fer-1 group: After 2 wk of exposure to hypoxia, the mice were injected with 1.5×10^5 HUCMSCs-LUC that were treated with Fer-1 (4 µM, 6 h) per mouse *via* the tail vein and then housed under hypoxia for 2 wk ($n = 6$); and HUCMSCs/sh-CSE + Fer-1 group: After 2 wk of exposure to hypoxia, the mice were injected with 1.5×10^5 HUCMSCs-LUC/sh-CSE that were treated with Fer-1 (4 µM, 6 h) per mouse *via* the tail vein and then housed under hypoxia for 2 wk ($n = 6$).

One day and seven days after intravenous injection *via* the tail, mice were anaesthetized using isoflurane and placed in an IVIS Lumina imaging station. Images of regions of interest were collected 10 min after the intraperitoneal injection of D-luciferin (L6152, Sigma-Aldrich, United States), the luciferase substrate, at 3.75 mg per 25 g mouse weight.

Measurement of pulmonary artery pressure and right ventricular hypertrophy

After 4 wk, the mice were anaesthetized using isoflurane for haemodynamic assessment. Briefly, a Miler catheter was used to obtain the right ventricular systolic pressure (RVSP) *via* insertion into the right external jugular vein. After exsanguination and collection of the blood, the cardiopulmonary tissues were removed. The right ventricle (RV) free wall and the left ventricle plus septum (LV + S) were weighed separately. The degree of right ventricular hypertrophy was determined by the ratio RV/(LV + S).

Assessment of pulmonary vascular morphometry

After the lung tissue was embedded in paraffin and cut into slices with a thickness of 5 µm, the slices were dewaxed, rehydrated, and stained with haematoxylin and eosin staining. Then, the ratio of the vascular medial cross-sectional area to the total arterial cross-sectional area was calculated as a measurement of distant small pulmonary artery (50-100 µm) remodelling.

For immunofluorescence staining of the lung tissue, after deparaffinization and washing with PBST, lung tissue slides were heated for 20 min at 95 °C in a Tris-EdTA solution for antigen retrieval and then blocked with 3% H₂O₂ for 15 min to block endogenous peroxidase activity and 5% goat serum for 1 h to eliminate nonspecific staining. These slides were incubated with VEcadherin rabbit polyclonal antibody (1:100, ab205336, Abcam) and alpha-smooth muscle actin rabbit monoclonal antibody (1:100, 19245S, CST) at 4 °C overnight and then incubated with the secondary antibody: Antirabbit immunoglobulin G (IgG) (1:500, 4413s, CST) or antirabbit IgG (1:500, 4412S, CST). Nuclei were counterstained with DAPI (D9542, Sigma-Aldrich, United States) at room temperature for another 2 min. Immunofluorescence was visualized under a microscope.

Analysis of cell apoptosis

After treatment, the cells were washed, trypsinized, resuspended, and stained with 5 µL of Annexin V/FITC (331200, Invitrogen, United States) and 5 µL of propidium iodide (PI, P1304MP, Invitrogen, United States) at room temperature for 15 min. Then, cell apoptosis was evaluated by flow cytometry.

Iron assays

Two different methods were used to measure the levels of intracellular ferrous iron. For a colorimetric method using the Iron Assay Kit (ab83366, Abcam, United Kingdom), cells were collected, homogenized (in cold iron assay buffer), and centrifuged. After adding 5 µL of iron reducer to each sample, the supernatant was incubated for 30 min at 37 °C. Next, 100 µL of iron probe was added to each sample and incubated for 60 min at 37 °C in the dark. The absorbance at 593 nm was measured using a microplate reader. For FeRhoNox-1 staining, cells were incubated away from light in a 37 °C, 5% CO₂ incubator for 40 min after the addition of 5 µM FeRhoNox-1 (MX4558, MKbio, CHN). Then, the cells were washed with PBS three times and imaged by fluorescence microscopy.

Reactive oxygen species assay

Intracellular reactive oxygen species (ROS) levels were measured by applying DCFH-DA (S0033, Beyotime, CHN). Briefly, after treatment, the cells were washed with PBS three times and treated with 10 µM DCFH-DA for 30 min away from light. Then, the cells were washed with PBS and observed under a fluorescence microscope.

Lipid peroxide measurement

Cells were labelled with BODIPY™ 581/591 C11 (D3861, Thermo Fisher Scientific, United States) at a final concentration of 2 µM for 20 min at 37 °C. After trypsinization and resuspension in PBS, lipid peroxidation was analysed using a flow cytometer. A lipid peroxidation [malonaldehyde (MDA)] assay (ab118970, Abcam, United Kingdom) was used according to the manufacturer's protocol to quantify the MDA concentration. The results were quantified colorimetrically (OD = 532 nm). The reduced glutathione/oxidized glutathione disulfide (GSH/GSSG) ratio in cells was determined using the GSH/GSSG Ratio Detection Assay Kit (ab205811, Abcam, United Kingdom) following the manufacturer's instructions.

Cystine uptake

Cystine uptake was measured with BioTracker Cystine-FITC Live Cell Dye (SCT047, Sigma-Aldrich, United States). The pretreated cells were incubated with complete medium containing 5 µM cystine-FITC in the dark for 30 min. Then, the cells were washed with PBS and harvested by trypsinization. The cells were resuspended in PBS and assessed by flow cytometry.

Transmission electron microscopy

Cells were fixed, postfixed, dehydrated, cut, and stained as previously described[15]. The cells were viewed under a transmission electron microscope (JEM1200, Tokyo, Japan), and images were taken.

Measurement of the H₂S concentration

The dye 7-azido-4-methylcoumarin (AzMC) was used to measure the H₂S concentration *in vitro*. Cells were plated at a density of 10000 cells per well in 96-well plates. After treatment, cells were loaded with the fluorogenic dye AzMC (802409, Sigma-Aldrich, United States) at 10 µM for 30 min. Then, the cells were washed three times with PBS and measured on a SpectraMax M5 plate reader.

Nrf2 activity assay

Nuclear lysates were isolated following extraction using NE-PER Nuclear and Cytoplasmic Extraction Reagents (78835, Thermo Fisher Scientific, United States) according to the manufacturer's instructions. Nrf2 transcriptional activity was then measured by ELISA using an Nrf2 Transcription Factor Assay Kit (ab207223, Abcam, United Kingdom) in accordance with the manufacturer's guidelines.

S-sulphydration assay

Kelch-like ECH-associating protein 1 (Keap1) S-sulphydration was detected with standard procedures using the "tag-switch" method[16]. The Keap1 protein was pulled down by immunoprecipitation. The proteins were dissolved in solution buffer, purified with streptavidin-agarose beads, and subjected to western blotting with anti-Keap1 (sc-365626, Santa Cruz Biotechnology, United States). Cells were treated with 1 mmol/L 1,4-dithio-DL-threitol (DTT, 43815, Sigma-Aldrich, United States) for 3 h as a negative control group.

Quantitative real-time polymerase chain reaction

qPCR was performed as previously described[15,17]. Human GAPDH expression was used for normalization. Fold changes were calculated using the comparative Ct method ($\Delta\Delta Ct$). The sequences of the primers used are as follows: CSE: Forward: GGCCTGGTGTCTGTAAATTGT and reverse: GCCATTCCGTTTTTGAAATGCT; GAPDH: forward: GACATCAAGAAGGTGGTGAAGCAGG and reverse: GTGTCGCTGTTGAAGTCAGAGGAGA.

Western blot analysis

Whole-cell, cytosolic, and nuclear proteins were extracted using RIPA Lysis and Extraction Buffer (89900, Thermo Fisher Scientific, United States) or NE-PER Nuclear and Cytoplasmic Extraction Reagents (78835, Thermo Fisher Scientific, United States). The extractions were performed as previously described[17]. Primary antibodies against the following were used: Glutathione peroxidase 4 (GPX4, 1:1000, 59735S, CST), intracellular ferritin heavy chain 1 (FTH1, 1:1000, 4393S, CST), nuclear receptor coactivator 4 (NOCA4, 1:1000, 66849S, CST), Fe³⁺-bound transferrin receptor 1 (TFRC1, 1:1000, ab214039, Abcam), 4-hydroxynonenal (4-HNE, 1:1000, ab46545, Abcam), SLC7A11 (1:1000, ab175186, Abcam), Nrf2 (1:1000, ab62352, Abcam), Keap1 (sc-365626, Santa Cruz Biotechnology), CSE (1:1000, 19689S, CST), GAPDH (1:1000, 5174S, CST), and Histone H3 (1:1000, ab1791, Abcam). The intensity of the resulting bands was analysed with ImageJ software.

Statistical analysis

All experimental data are presented as the mean \pm SEM. Statistical significance was analysed with GraphPad Prism version 5.01 (San Diego, CA, United States) using one-way analysis of variance (ANOVA). Differences at $P < 0.05$ were considered statistically significant. All experiments were performed with at least three independent replicates.

RESULTS

In vitro assessment of HUCMSCs

HUCMSCs-LUC were analysed *in vitro* by bioluminescence imaging (BLI), cell morphology assessment, flow cytometry, and differentiation potential determination to confirm the properties typical of HUCMSCs. A linear relationship between the number of cells and the bioluminescent signal was observed (Figure 1A). Cells displayed a spindle-like shape and were arranged in radial concentric circles (Figure 1B). Adipogenic and osteogenic differentiation confirmed the multipotentiality and differentiation capacity of the HUCMSCs-LUC (Figure 1B). Flow cytometry confirmed the presence of the following stem cell-specific molecules on the cell surface: CD90 in 94.25% of the cells, CD73 in 83.35%, CD105 in 90.18%, CD44 in 82.16%, CD34 in 0.21%, CD45 in 0.45%, and HLA-DR in 1.36% (Figure 1C).

Ferroptosis could be induced in HUCMSCs

To verify whether ferroptosis could be induced in HUCMSCs and to ascertain the optimal concentration and time, HUCMSCs were exposed to increasing doses (1 μ M, 2 μ M, 3 μ M, 4 μ M, and 5 μ M) of erastin, a ferroptosis inducer, for three different durations (12 h, 24 h, and 48 h). As shown in Figures 2A-C, the CCK-8 assay illustrated that compared to that in untreated cells, cellular viability was notably reduced to 50% by erastin treatment at concentrations greater than 3 μ M for less than 24 h of exposure. In addition, because cell membrane structures can be destroyed by ferroptosis, which leads to the release of LDH from the cytoplasm into the culture medium[18], the levels of LDH in the supernatant were monitored after treatment with increasing erastin concentrations for 12 h, 24 h, and 48 h (Figures 2E-G). The results showed that LDH release increased in a time- and dose-dependent manner. Similarly, treatment with erastin at a concentration greater than 3 μ M for 24 h significantly increased LDH release to about 50% compared with that of the untreated HUCMSCs. Thus, HUCMSCs were treated with erastin at a concentration of 3 μ M for 24 h in subsequent experiments.

Fer-1 was used to determine whether ferroptosis inhibition could protect HUCMSCs from erastin-induced cell death. Erastin-treated HUCMSCs were cotreated with Fer-1 at concentrations of 0, 2, 4, 6, and 8 μ M for 24 h. As shown in Figures 2D and H, Fer-1 above 4 μ M had a significant protective effect over treatment without Fer-1.

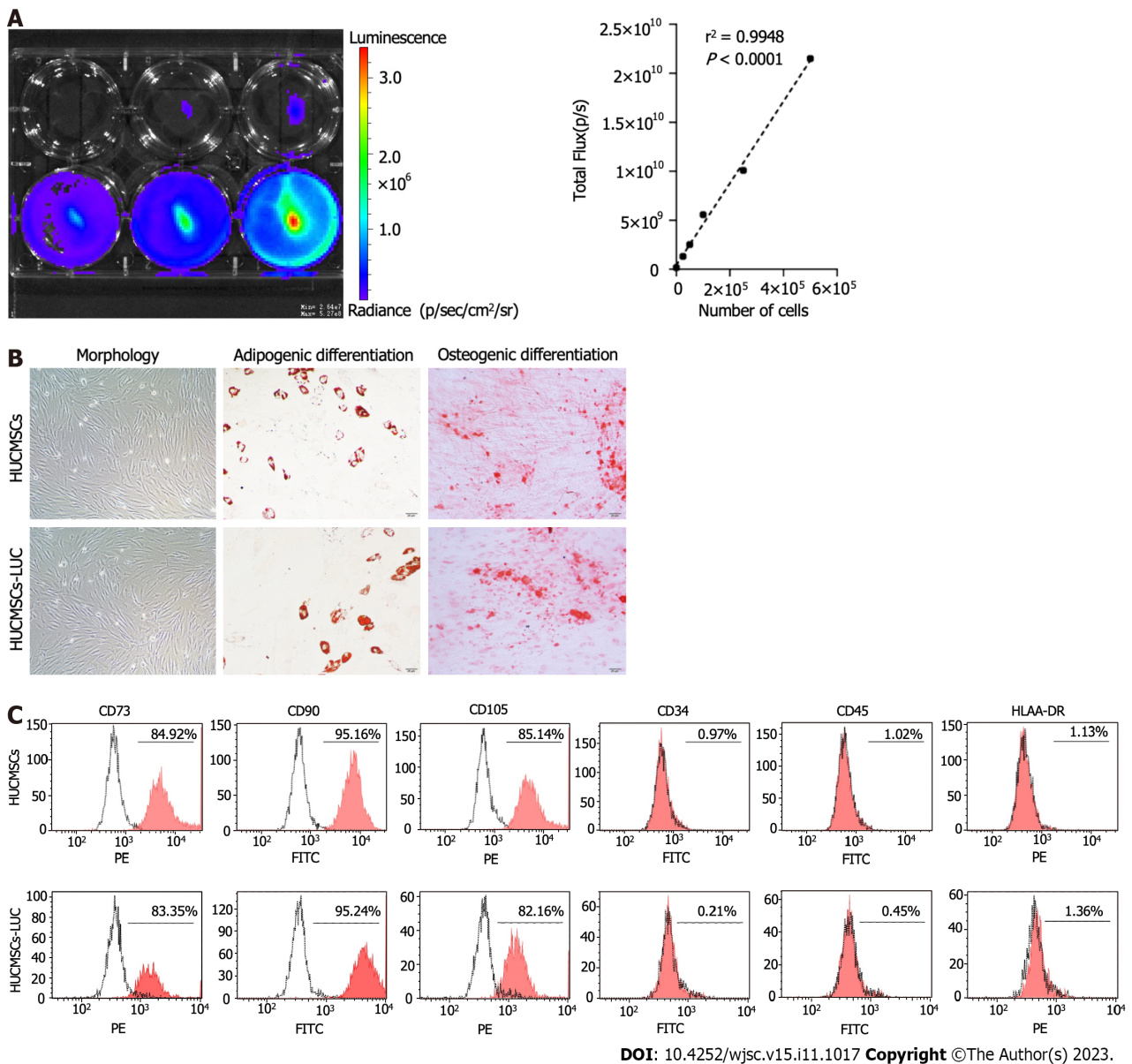


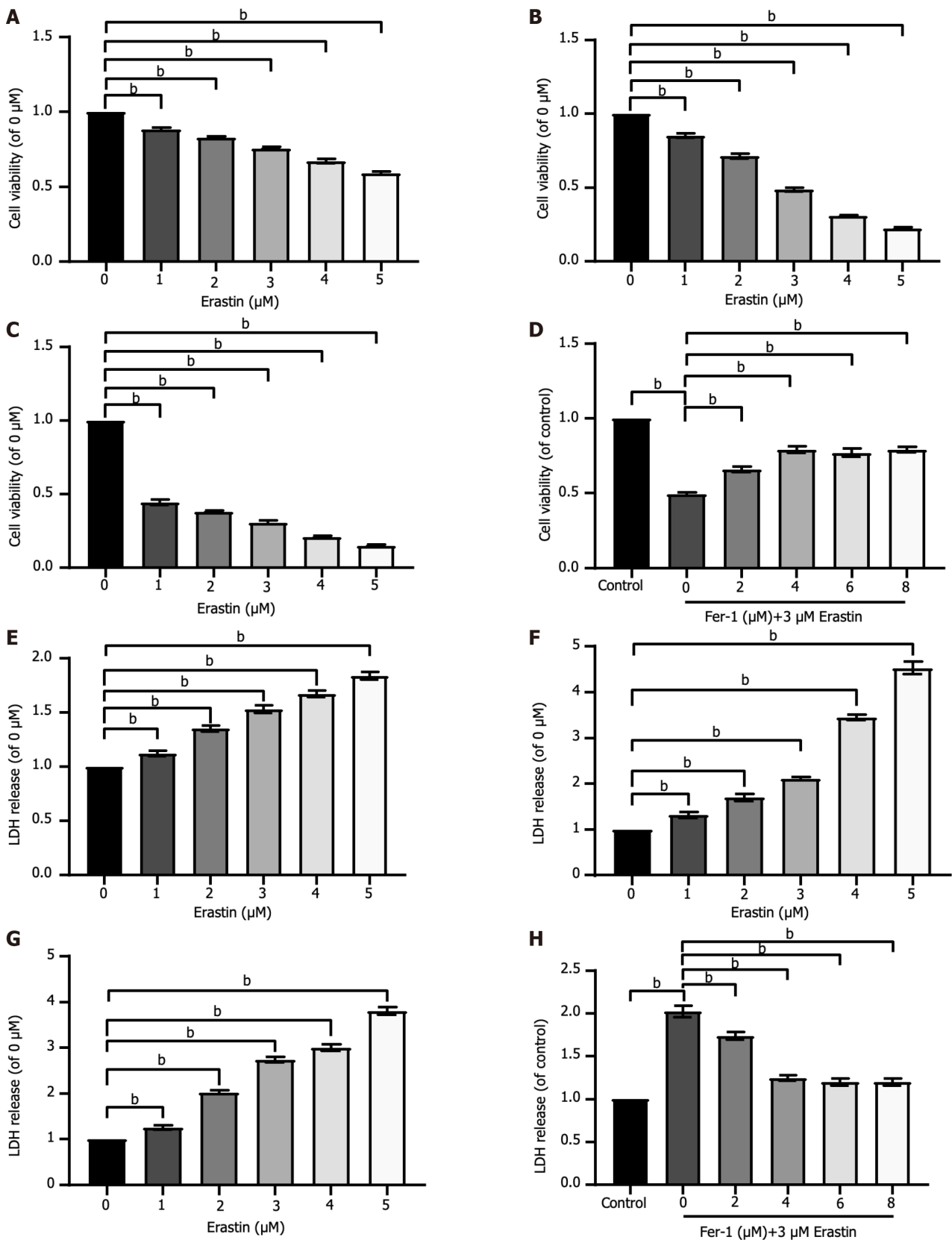
Figure 1 Characteristics of human umbilical cord mesenchymal stem cells expressing firefly luciferase gene. A: Luciferase activity of human umbilical cord mesenchymal stem cells expressing firefly luciferase gene (HUCMSCs-LUC). Representative luciferase imaging is shown using *in vivo* imaging system; B: Morphologies of HUCMSCs-LUC. HUCMSCs-LUC differentiated into adipocytes (stained with oil red O for lipid droplets) and osteocytes (stained with alizaline red for mineral deposition); C: Surface marker expression of HUCMSCs-LUC in flow cytometry analysis. HUCMSCs: Human umbilical cord mesenchymal stem cells; HUCMSCs-LUC: Human umbilical cord mesenchymal stem cells expressing firefly luciferase gene; PE: Phycoerythrin; FITC: Fluorescein isothiocyanate.

Longitudinal *in vivo* BLI of HUCMSC grafts

After 1.5×10^5 HUCMSCs-LUC were grafted in each mouse, longitudinal *in vivo* BLI was performed on day 1 post-implantation. For quantitative analysis of the observed BLI signals, cell graft-specific BLI signals from fixed regions on the mouse chest and the mean background BLI signals from fixed control regions on the mouse head were plotted *vs* time post-implantation (Figure 3A). The BLI signal was decreased in the HUCMSCs + erastin group and increased in the HUCMSCs + Fer-1 group compared to the HUCMSCs group (Figure 3B). In addition, the signal was further increased in the HUCMSCs/CSE + erastin group but decreased in the HUCMSCs/sh-CSE + Fer-1 group (Figure 3B).

Pulmonary artery remodelling in each group

In PAH, pulmonary artery remodelling results in progressively elevated pulmonary arterial pressure, which ultimately leads to right heart failure[19]. As shown in Figures 3C, F, G, and I, the administration of HUCMSCs or HUCMSCs + Fer-1 decreased the RVSP and RV/(LV + S) ratio in mice with hypoxia-induced PAH ($P < 0.01$). Interestingly, compared to those in the HUCMSCs group, the RVSP and RV/(LV + S) decreased to a greater extent in the HUCMSCs + Fer-1 group (17.000 ± 2.215 *vs* 22.280 ± 3.115 , 23.376 ± 0.537 *vs* 28.781 ± 2.311 , both $P < 0.01$) and increased in the HUCMSCs + erastin group (34.363 ± 4.065 *vs* 22.280 ± 3.115 , 39.158 ± 0.809 *vs* 28.781 ± 2.311 , both $P < 0.01$). Moreover, compared to those in the HUCMSCs + erastin group, the RVSP and RV/(LV + S) were decreased in the HUCMSCs/CSE + erastin group (25.817 ± 2.843 *vs* 34.363 ± 4.065 , 33.082 ± 2.405 *vs* 39.158 ± 0.809 , both $P < 0.01$). Furthermore, the RVSP and RV/(LV + S) were



DOI: 10.4252/wjsc.v15.i11.1017 Copyright ©The Author(s) 2023.

Figure 2 Ferroptosis exists in human umbilical cord mesenchymal stem cells. A-C: Cell viability was assessed after exposure to different concentrations of erastin for different times (12 h, 24 h, and 48 h); D: Cell viability was assessed after exposure to 3 μM erastin and different concentrations of ferrostatin-1 (Fer-1). Cell viability was measured with Cell Counting Kit-8 kit; E-G: Lactic dehydrogenase (LDH) release was assessed after exposure to different concentrations of erastin for different times (12 h, 24 h, and 48 h); H: LDH release was assessed after exposure to 3 μM erastin and different concentrations of Fer-1. LDH release was measured with LDH cytotoxicity detection kit. The data were from at least three independent experiments. Data were quantified for cells subjected to erastin (0 μM), and values are represented as the mean \pm SD. Fer-1: Ferrostatin-1; LDH: Lactic dehydrogenase. ^b*P* < 0.01.

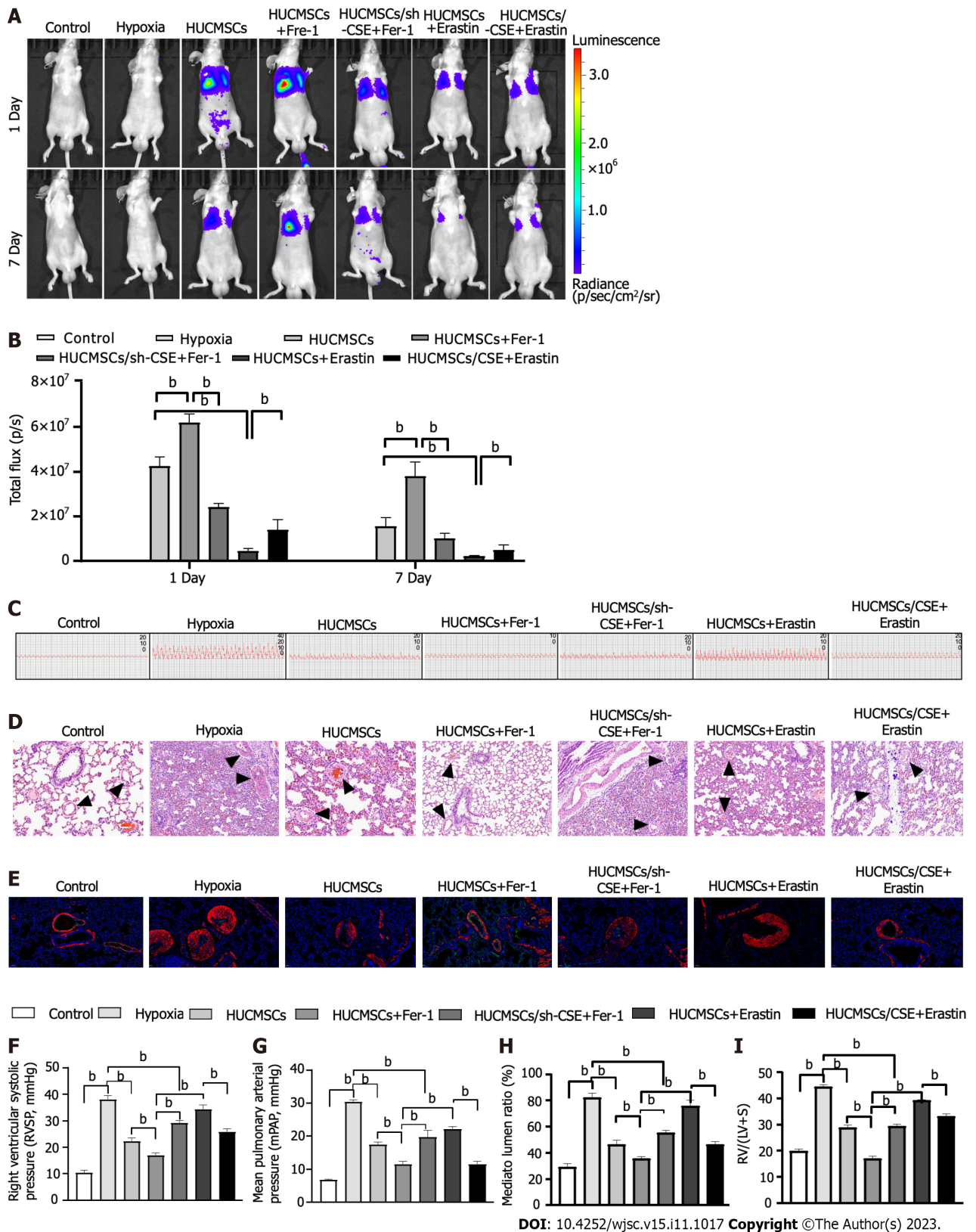
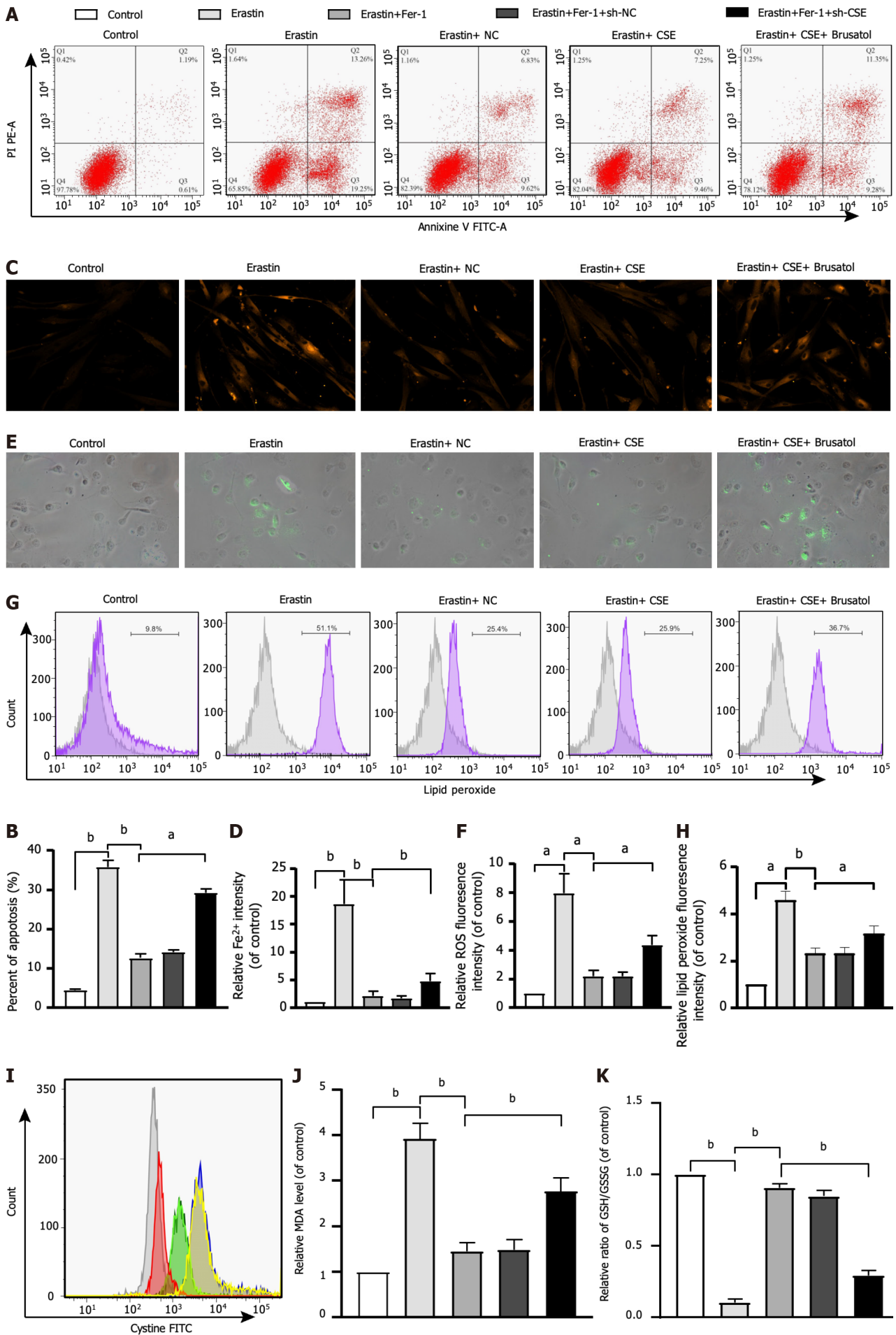


Figure 3 Change of pulmonary arterial remodeling. A: *In vivo* bioluminescence imaging (BLI). Representative time course image showing *in vivo* BLI of mice grafted with living human umbilical cord mesenchymal stem cells expressing firefly luciferase gene in the lungs. Images were acquired at 24 h and 7 d post-implantation. Regions of interest are drawn on the mouse lung and on the mouse shoulder, considered as background signal; B: *In vivo* BLI. Quantitative analysis of *in vivo* BLI at days 1 and 7 post-implantation; C-H: Representing pulmonary arterial pressure (C, F, and G). Representative haematoxylin and eosin-stained lung sections and quantification of the ratio of the medial wall area to the total vessel cross sectional area of the distal pulmonary artery sections (D and H). Immunofluorescent staining (E). Green fluorescence represents VEcadherin, red fluorescence represents alpha-smooth muscle actin, and blue fluorescence indicates 4',6-diamidino-2-phenylindole nuclear staining; I: Right ventricle/left ventricle plus septum. Data are expressed as the mean \pm SEM ($n = 6$ /group). HUCMSCs: Human umbilical cord mesenchymal stem cells; Fer-1: Ferrostatin-1; CSE: Cystathionine γ -lyase; RV/(LV + S): Right ventricle/(left ventricle plus septum). ^b $P < 0.01$.



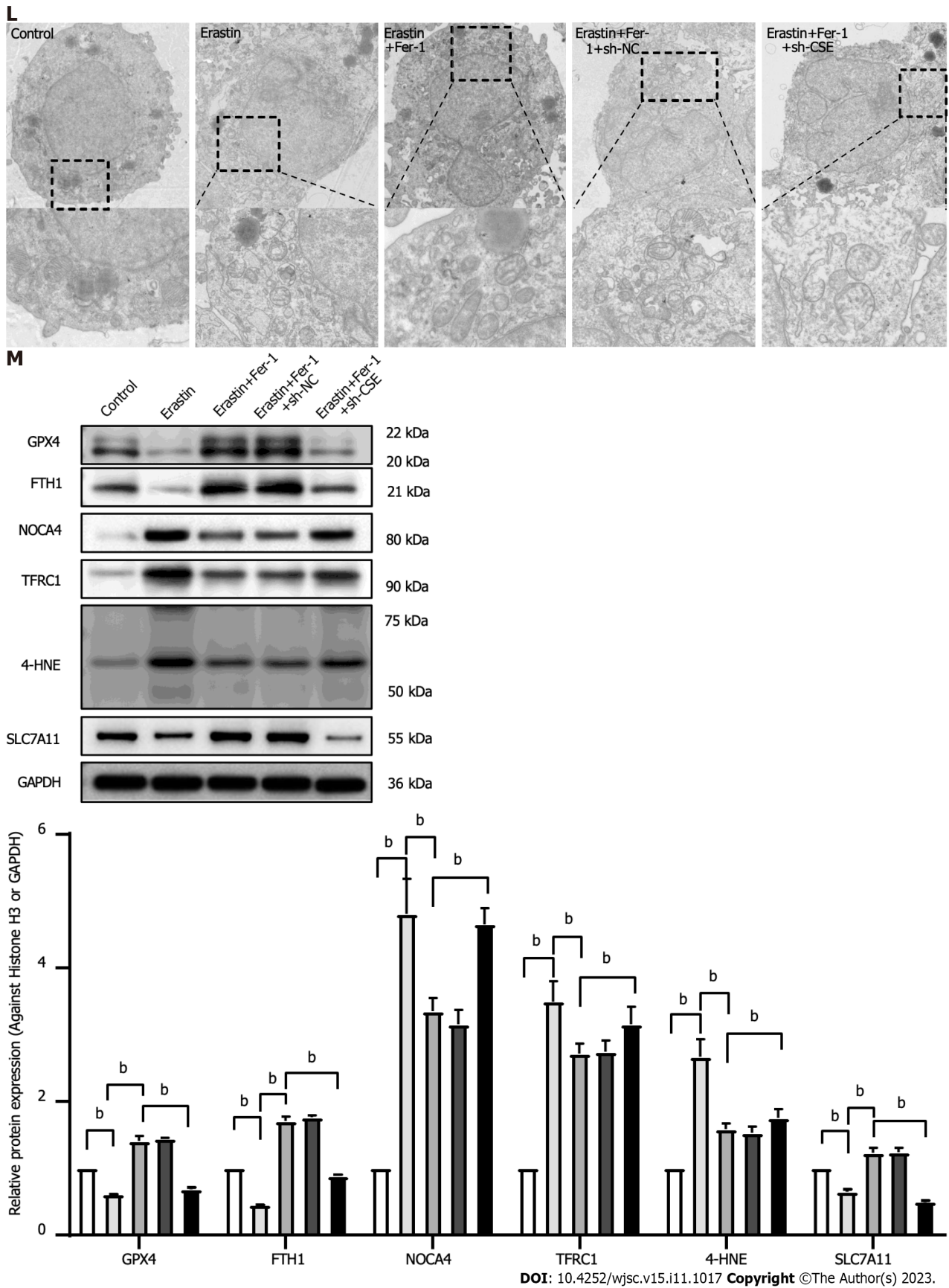


Figure 4 Effect of cystathionine γ -lyase overexpression on ferroptosis in human umbilical cord mesenchymal stem cells. A and B: Cell apoptosis was analyzed by Annexin V-fluorescein isothiocyanate (FITC)/propidine iodide staining using flow cytometry analysis ($n = 3$), and quantified on the basis of apoptosis rate ($n = 3$); C and D: Iron level was detected by FeRhoNox-1 staining (C) and iron assay kit (D); E and F: Immunofluorescent staining of total reactive oxygen species; G and H: Level of lipid peroxidation detected by flow cytometry analysis after staining with C11-BODIPY; I: Intracellular cystine-FITC levels measured by flow cytometry. Results represent three independent experiments; J: Malonaldehyde level; K: Ratio of reduced glutathione/oxidized glutathione disulfide;

L: Mitochondrial morphological changes detected by transmission electron microscopy; M: Western blot analysis of expression of the glutathione-dependent antioxidant enzyme glutathione peroxidase, ferritin heavy chain 1, nuclear receptor coactivator 4, Fe³⁺-bound transferrin receptor 1, 4-hydroxynonenal, and SLC7A11 protein. Glyceraldehyde-3-phosphate dehydrogenase was used for normalization for protein ($n = 3$). Fer-1: Ferrostatin-1; Annexin V-FITC/PI: Annexin V-fluorescein isothiocyanate/propidium iodide; ROS: Reactive oxygen species; sh-CSE: Short hairpin RNA targeting cystathionine γ -lyase; MDA: Malonaldehyde; GSH/GSSG: Reduced glutathione/oxidized glutathione disulfide; GPX4: Glutathione-dependent antioxidant enzyme glutathione peroxidase; FTH1: Ferritin heavy chain 1; NCOA4: Nuclear receptor coactivator 4; TFRC1: Fe³⁺-bound transferrin receptor 1; 4-HNE: 4-hydroxynonenal; GAPDH: Glyceraldehyde-3-phosphate dehydrogenase. ^a $P < 0.05$, ^b $P < 0.01$.

increased in the HUCMSCs/sh-CSE + Fer-1 group compared with those in the HUCMSCs + Fer-1 group (29.232 ± 2.333 vs 17.000 ± 2.215 , 29.820 ± 1.526 vs 23.376 ± 0.537 , both $P < 0.01$).

Endothelial to mesenchymal transition (EnMT) has been causally linked to pulmonary arterial remodelling in PAH[20, 21]. EnMT is a form of cellular plasticity described as a phenotypic conversion whereby endothelial cells lose endothelial characteristics (CD31 expression) and acquire mesenchymal characteristics (VE-cadherin expression)[22]. Here, as shown in Figures 3D, E and H, histological and immunofluorescence staining showed slight pulmonary artery stenosis and EnMT in the groups exposed to hypoxia, and these effects were largely attenuated by treatment with HUCMSCs and HUCMSCs + Fer-1 ($P < 0.01$). Interestingly, the inhibitory effect of HUCMSCs + Fer-1 on small pulmonary artery stenosis and EnMT was stronger than that of HUCMSCs. In addition, compared to those in the HUCMSCs + erastin group, small pulmonary artery stenosis and EnMT were alleviated in the HUCMSCs/CSE + erastin group ($P < 0.01$). Meanwhile, small pulmonary artery stenosis and EnMT were aggravated in the HUCMSCs/sh-CSE group compared with the HUCMSCs/Fer-1 group ($P < 0.05$).

CSE inhibition exacerbates Fer-1-mediated suppression of ferroptosis in HUCMSCs

We observed ferroptosis-related changes in erastin-treated HUCMSCs. As shown in Figure 4, cell apoptosis; the levels of Fe²⁺, ROS, lipid peroxidation, and MDA; and the expression of 4-HNE, TFRC1, and NOCA4 were significantly increased, while the GSH/GSSG ratio; cystine uptake; and GPX4, FTH1, and SLC7A11 expression were decreased in the erastin group compared with the control group (all $P < 0.05$). Consistent with these results, transmission electron microscopy (TEM) also showed an increased mitochondrial membrane density and shorter mitochondrial cristae in the erastin group (Figure 4L). Moreover, the above changes in erastin-treated HUCMSCs were reversed by Fer-1 administration (all $P < 0.05$). Interestingly, the inhibitory effect of Fer-1 on ferroptosis was aggravated by CSE inhibition (all $P < 0.05$).

CSE overexpression negatively regulates erastin-induced ferroptosis in HUCMSCs

As shown in Figure 5, there was a significant decrease in cell apoptosis; the levels of Fe²⁺, ROS, lipid peroxidation, and MDA; and the expression of 4-HNE, TFRC1, and NOCA4, whereas there was an increase in the GSH/GSSG ratio; cystine uptake; and the expression of GPX4, FTH1, and SLC7A11 in the erastin + CSE group compared to the erastin group (all $P < 0.05$). Consistent with these results, TEM also showed that the mitochondrial membrane was intact and that the mitochondria were narrower with an increased number of cristae in the erastin + CSE group (Figure 5L). In addition, the inhibitory effect of CSE overexpression on ferroptosis was abolished by brusatol, an Nrf2 inhibitor (all $P < 0.05$).

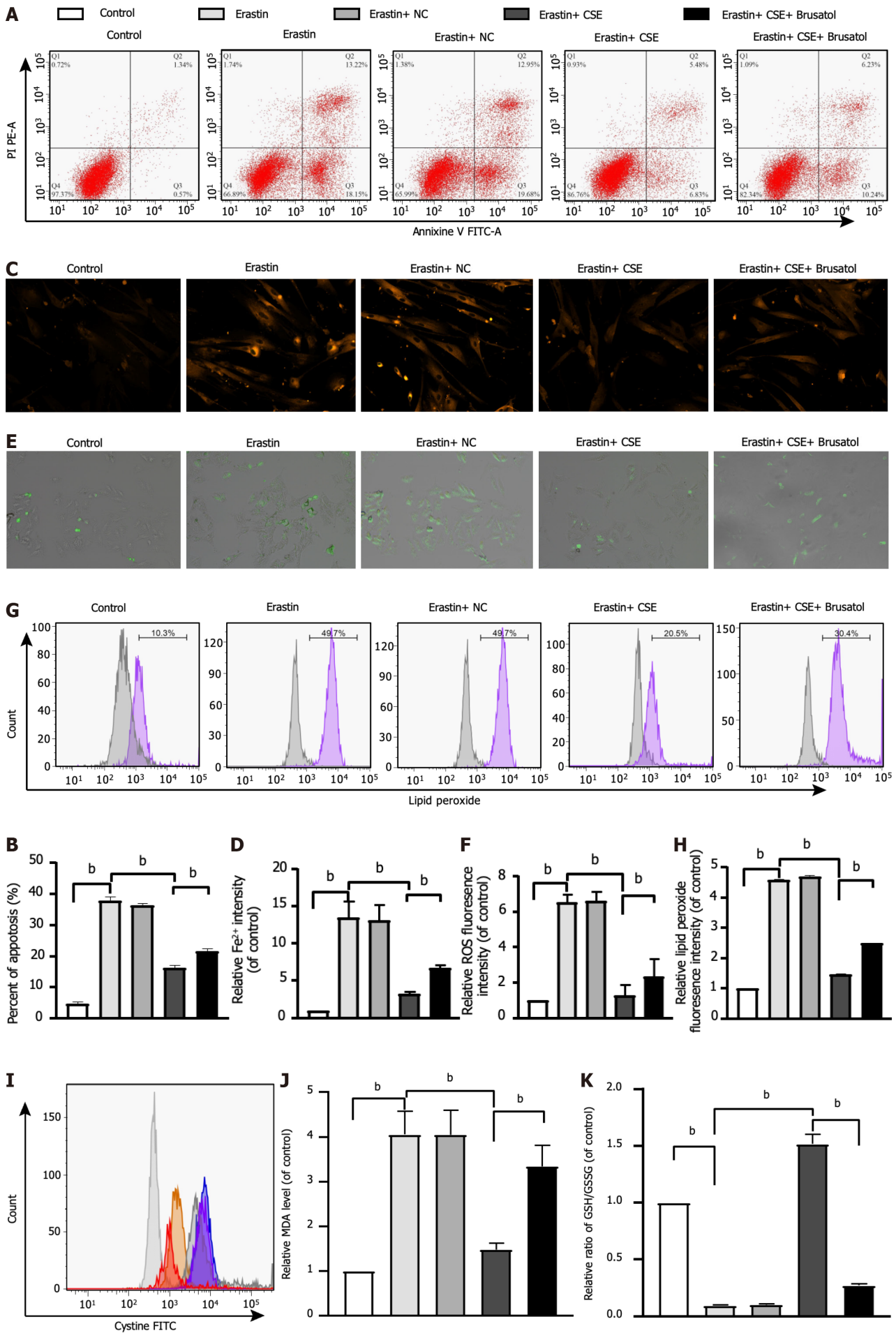
The CSE/H₂S pathway induces Keap1 S-sulphydration and nuclear translocation of Nrf2

We examined whether Nrf2 is involved in the protective effect of the CSE/H₂S pathway against the ferroptosis of HUCMSCs. First, we found that CSE inhibition decreased H₂S production (Figure 6A), while CSE overexpression increased H₂S levels in HUCMSCs (Figure 6B). In addition, CSE inhibition further downregulated Fer-1-induced Nrf2 activation (Figure 6C), while CSE overexpression further upregulated erastin-induced Nrf2 inactivation (Figure 6D).

Then, the expression of Nrf2 was examined. Western blot analysis revealed that erastin treatment significantly inhibited Nrf2 nuclear translocation, and this effect was markedly enhanced when erastin treatment was combined with Fer-1 treatment (Figure 6E). Moreover, CSE inhibition upregulated Nrf2 expression in the cytoplasm and downregulated Nrf2 expression in the nucleus (Figure 6E). In contrast, CSE overexpression increased nuclear Nrf2 expression and decreased cytoplasmic Nrf2 expression (Figure 6F).

Next, we found that CSE overexpression-induced ferroptosis inhibition was successfully abolished by treatment with 10 nM brusatol, an Nrf2 inhibitor, for 6 h in HUCSMCs (Figure 6F). We also found no difference in the expression of Keap1 among the groups (Figures 6E and F).

Finally, with the "tag-switch" assay, the S-sulphydration of Keap1 was tested. S-sulphydration is a novel posttranslational modification involving H₂S. However, S-sulphydration, a covalent modification, can be reversed by DDT. Increased S-sulphydration of Keap1 was found in the HUCMSCs/CSE + erastin group than in the HUCMSCs + erastin group, and decreased S-sulphydration of Keap1 was detected in the HUCMSCs/sh-CSE + Fer-1 group than in the HUCMSCs + Fer-1 group (Figure 6G). Moreover, the S-sulphydration of Keap1 was further decreased after treatment with DTT, which indicated that Keap1 is S-sulphydrated (Figure 6G). As shown in Figure 6H, S- of Keap1 led to decreased nuclear Nrf2 expression, which indicated that the activation of Nrf2 by the CSE/H₂S pathway is dependent on Keap1 S-sulphydration in HUCMSCs.



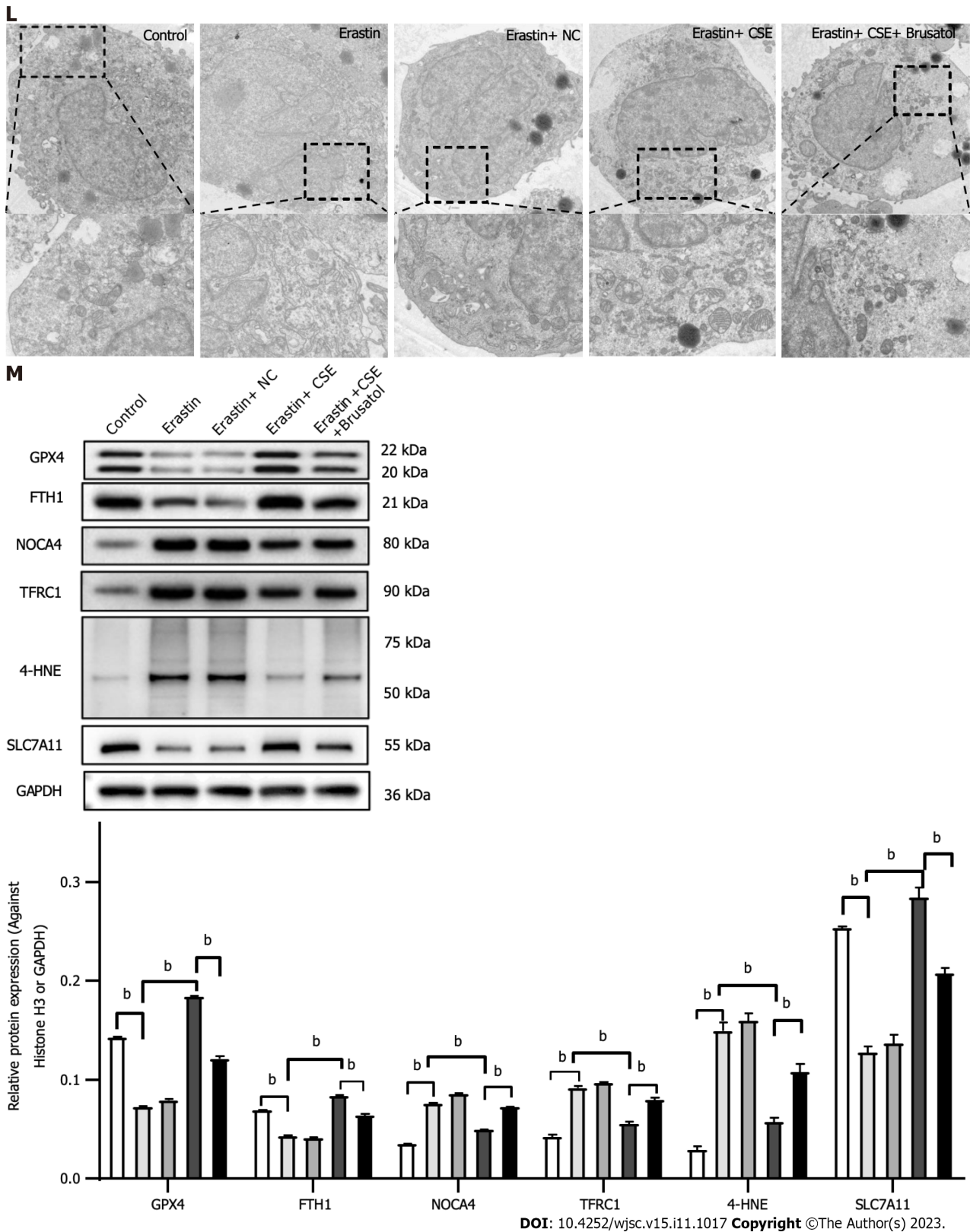


Figure 5 Effect of cystathionine γ -lyase inhibition on ferroptosis in human umbilical cord mesenchymal stem cells. A and B: Cell apoptosis was analyzed by Annexin V-fluorescein isothiocyanate (FITC)/propidine iodide staining using FACS ($n = 3$), and quantified on the basis of apoptosis rate ($n = 3$); C and D: Iron level detected by FeRhoNox-1 staining (C) and iron assay kit (D); E and F: Immunofluorescent staining of total reactive oxygen species; G and H: Level of lipid peroxidation detected by flow cytometry after staining with C11-BODIPY; I: Intracellular cystine-FITC levels measured by flow cytometry. Results represent three independent experiments; J: Malonaldehyde level; K: Ratio of reduced glutathione/oxidized glutathione disulfide; L: Mitochondrial morphological changes detected by transmission electron microscopy; M: Western blot analysis of expression of glutathione-dependent antioxidant enzyme glutathione peroxidase, ferritin heavy chain 1, nuclear receptor coactivator 4, Fe³⁺-bound transferrin receptor 1, 4-hydroxynonenal, and SLC7A11 protein. Glyceraldehyde-3-phosphate dehydrogenase was used for normalization for protein ($n = 3$). Fer-1: Ferrostatin-1; Annexin V-FITC/PI: Annexin V-fluorescein isothiocyanate/propidine iodide; ROS: Reactive oxygen species;

MDA: Malonaldehyde; CSE: Cystathionine γ -lyase; GSH/GSSG: Reduced glutathione/oxidized glutathione disulfide; GPX4: Glutathione-dependent antioxidant enzyme glutathione peroxidase; FTH1: Ferritin heavy chain 1; NCOA4: Nuclear receptor coactivator 4; TFRC1: Fe³⁺-bound transferrin receptor 1; 4-HNE: 4-hydroxynonenal; GAPDH: Glyceraldehyde-3-phosphate dehydrogenase. ^b*P* < 0.01.

DISCUSSION

Ferroptosis has been reported as a form of cell death; however, to date, understanding the potential effects of ferroptosis on MSC delivery requires further investigation. In the present study, we showed that ferroptosis occurred during HUCMSC delivery in mice with hypoxia-induced PAH. Moreover, mediation of the CSE/H₂S pathway suppressed ferroptosis in HUCMSCs.

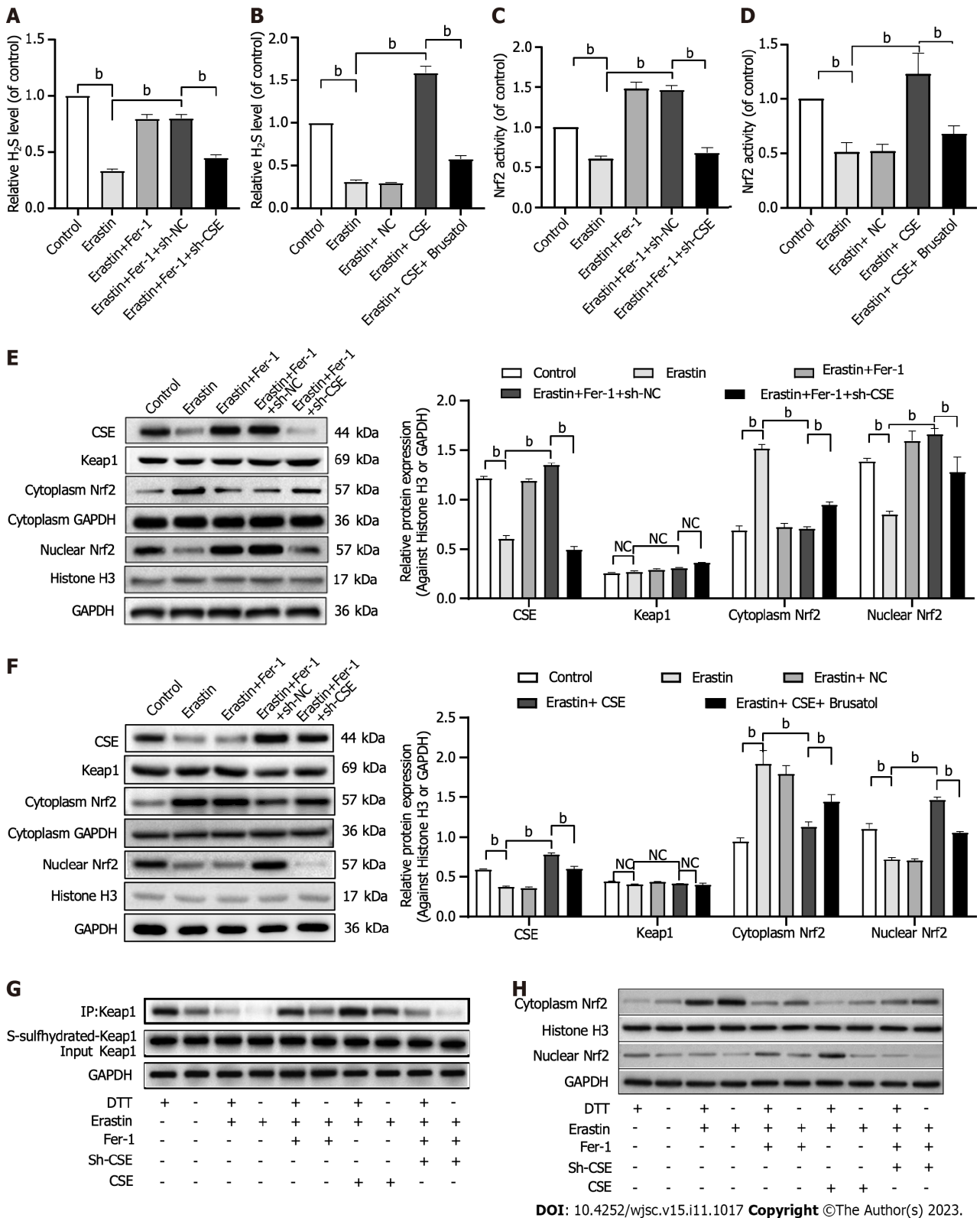
A desirable advantage of MSCs is their ability to home to damaged tissue sites. Evidence has demonstrated that transplanted MSCs can accumulate in lung tissue, inhibit vascular remodelling, and effectively attenuate pulmonary hypertension. In the present study, HUCMSCs were chosen because of their many characteristics, which include their ability to be extracted *via* a noninvasive procedure and high differentiation potential, the ease of their *in vitro* expansion, and their prominent repair properties. To detect transplanted HUCMSCs *in vivo*, HUCMSCs were labelled with firefly luciferase by transduction with a lentiviral vector. Furthermore, we determined that the surface markers and differentiation potential of the HUCMSCs were not disrupted after transduction. In this study, we monitored the survival of HUCMSCs in lung tissue 1 d and 7 d after intravenous injection and found that the HUCMSCs homed to injured lung tissue. Moreover, our data indicated the protective roles of HUCMSCs against pulmonary artery remodelling in mice under hypoxia.

Although MSCs can reach impaired sites due to their homing capacity, cell survival in these places is rare. At present, many potential methods to reduce MSC fate *in vivo* have been identified, including drug pretreatment, genetic modification, and preconditioning. However, our study indicated that pretreatment with Fer-1, an inhibitor of ferroptosis, increased HUCMSC survival in the lung, and combined treatment of HUCMSCs with Fer-1 further decreased vascular remodelling in mice with PAH. Conversely, worse cell survival and decreased therapeutic effects were detected in PAH mice after the delivery of HUCMSCs pretreated with erastin, which induces ferroptosis. Thus, the results showed that ferroptosis may have been linked to HUCMSCs survival in mice with hypoxia-induced PAH.

Researchers have indicated that ferroptosis can be activated by iron overload or the inactivation of GPX4[23-25]. During ferroptosis, following its import through TFRC1, Fe³⁺ is catalysed and converted to Fe²⁺ in the cytoplasm, which then participates in the Fenton reaction, causing ferroptosis. Moreover, Fe²⁺ also binds intracellular FTH1, which can be transported to lysosomes by NCOA4, leading to intracellular iron overload. However, GPX4 is the major endogenous factor that reduces lipid peroxidation[26]. Cystine is converted to cysteine by the cystine/glutamate antiporter system (Xc⁻), which generates GSH, a cofactor for GPX4[27,28]. In addition, the inhibition of SLC7A11, a key component of system Xc⁻, initiates ferroptosis[29], and MDA and 4-HNE, which are byproducts of lipid peroxidation, represent stable markers of oxidative stress that are also associated with ferroptosis[30]. In the present *in vitro* experiments, after Fer-1 administration, we detected decreased cell death, the rebalancing of intracellular iron homeostasis, and reduced levels of lipid peroxidation products, indicating that ferroptosis was suppressed by Fer-1 in erastin-treated HUCMSCs. This is consistent with the ability of Fer-1 and erastin to induce and inhibit ferroptosis, respectively[31].

On the basis of our *in vitro* and *in vivo* experimental results, we suggest that the CSE/H₂S pathway mediates ferroptosis in HUCMSCs. Synthesized by CSE in mammalian cells, H₂S has been shown to directly scavenge ROS[32], facilitate GSH production[33], inhibit GPX4 inactivation[34], and enhance the activity of system Xc[35], mitigating ferroptosis. Indeed, in our study, CSE inhibition decreased endogenous H₂S levels and exacerbated ferroptosis in HUCMSCs, while CSE overexpression increased intracellular H₂S production and inhibited ferroptosis in HUCMSCs. Although emerging evidence has shown that Nrf2 is among the major cellular defences against ferroptosis as it promotes the translation of antioxidant genes, such as FTH1[36], GPX4[37], and Xc[38], the effects of the CSE/H₂S pathway on Nrf2 activation in HUCMSCs have not been described. In our investigation, it was apparent that upregulation of the CSE/H₂S pathway promoted the translocation of Nrf2 into the nucleus, which indicated that Nrf2 was activated. In addition, using an Nrf2 inhibitor, we demonstrated that the inhibitory effects of the CSE/H₂S pathway against ferroptosis were mediated through the activation of Nrf2. Interestingly, we also found that the inactivation of Nrf2, in turn, led to the downregulation of CSE, which may have been caused by excessive oxidative stress-induced oxidation of CSE.

Keap1 is known to bind Nrf2 in the cytoplasm and inhibit it, preventing Nrf2 translocation to the nucleus. Under oxidative stress, the dissociation of Keap1 and Nrf2 results in the entrance of Nrf2 into the nucleus, where it initiates gene transcription[39]. In this study, we found that the CSE/H₂S pathway had little effect on total Keap1 protein expression in HUCMSCs. Thus, to further explore the mechanism underlying the effects of the CSE/H₂S pathway on Nrf2 activation, Keap1 S-sulfhydration was investigated in HUCMSCs. S-sulfhydration is a posttranslational modification induced by H₂S that leads to the attachment of sulfhydryl groups to selective proteins, yielding a hydropersulfide moiety (-SSH)[40]. However, the covalent modification that occurs in sulfhydration is reversible by DTT[40]. Recent publications have revealed that H₂S induces the S-sulfhydration of transcription factors, such as Keap1[41]. In this study, we found that Keap1 S-sulfhydration was inhibited upon ferroptosis. By comparing the difference in Keap1 S-sulfhydration between the HUCMSCs/CSE and HUCMSCs/sh-CSE groups, we demonstrated the significant role of Keap1 S-sulfhydration in the protective effects of the CSE/H₂S pathway against ferroptosis in HUCMSCs.



DOI: 10.4252/wjsc.v15.i11.1017 Copyright ©The Author(s) 2023.

Figure 6 Effect of cystathionine γ-lyase/hydrogen sulfide pathway on nuclear factor erythroid 2-related factor 2 activation and ferroptosis in human umbilical cord mesenchymal stem cells. A and B: Exogenous hydrogen sulfide (H₂S) production; C and D: Nuclear factor erythroid 2-related factor 2 (Nrf2) activity; E and F: Western blot analysis and quantification of cystathionine γ-lyase (CSE) protein, Kelch-like ECH-associated protein 1 (Keap1), and cytoplasmic and nuclear Nrf2 protein; G: Change of Keap1 S-sulfhydration. 1,4-Dithio-DL-threitol (DTT, 1 mmol/L, 3 h) served as a negative control; H: Effect of DTT on cytoplasmic and nuclear Nrf2 expression. Histone H3 was used for normalization for nuclear proteins, and glyceraldehyde-3-phosphate dehydrogenase was used for normalization for whole and cytoplasmic protein (n = 3). CSE: Cystathionine γ-lyase; H₂S: Hydrogen sulfide; Nrf2: Nuclear factor erythroid 2-related factor 2; HUCMSCs: Human umbilical cord mesenchymal stem cells; Fer-1: Ferrostatin-1; sh-CSE: Short hairpin RNA targeting cystathionine γ-lyase; Keap1: Kelch-like ECH-associated protein 1; DTT: 1,4-Dithio-DL-threitol; GAPDH: Glyceraldehyde-3-phosphate dehydrogenase. ^bP < 0.01.

CONCLUSION

In conclusion, the present data provide evidence for the first time that inhibiting ferroptosis improves the survival of HUCMSC transplanted in mice with hypoxia-induced PAH. Moreover, ferroptosis can be suppressed by regulating the CSE/H₂S pathway *via* S-sulfhydrated Keap1/Nrf2 signalling in HUCMSCs. Collectively, the ability of CSE to inhibit ferroptosis suggests that genetic approaches to manipulate CSE expression and H₂S production may provide a novel therapeutic avenue for improving the protective capacity of transplanted MSCs in PAH.

ARTICLE HIGHLIGHTS

Research background

Ferroptosis can decrease retention and engraftment after mesenchymal stem cell (MSC) delivery, which is considered a major challenge to the effectiveness of MSC-based therapy for pulmonary arterial hypertension (PAH). Interestingly, the cystathionine γ -lyase (CSE)/hydrogen sulfide (H₂S) pathway may contribute to mediating ferroptosis.

Research motivation

We aimed to investigate the influence of the CSE/H₂S pathway on ferroptosis in human umbilical cord MSCs (HUCMSCs).

Research objectives

We aimed to clarify whether the effect of HUCMSCs on vascular remodelling in mice with PAH is by CSE/H₂S pathway-mediated ferroptosis. Furthermore, the effect of the CSE/H₂S pathway on ferroptosis in HUCMSCs and the underlying mechanisms were investigated.

Research methods

Erastin and ferrostatin-1 (Fer-1) were used to induce and inhibit ferroptosis, respectively. HUCMSCs were transfected with a vector that overexpressed or inhibited CSE. A PAH mouse model was established using 4-wk-old male BALB/c nude mice under hypoxic conditions, and pulmonary pressure and vascular remodelling were measured. The survival of HUCMSCs after delivery was observed by *in vivo* bioluminescence imaging. Cell viability, iron accumulation, reactive oxygen species (ROS) production, cystine uptake, and lipid peroxidation in HUCMSCs were tested. Ferroptosis-related proteins and S-sulfhydrated Kelch-like ECH-associating protein 1 (Keap1) were detected by western blot analysis.

Research results

In vivo, CSE overexpression improved cell survival after erastin-treated HUCMSCs were delivered to mice with hypoxia-induced PAH. *In vitro*, CSE overexpression improved H₂S production and ferroptosis-related indexes in erastin-treated HUCMSCs, such as cell viability, the iron level, ROS production, cystine uptake, lipid peroxidation, mitochondrial membrane density, and ferroptosis-related protein expression. In contrast, *in vivo*, CSE inhibition decreased cell survival after Fer-1-treated HUCMSC delivery and aggravated vascular remodelling in the PAH mice. *In vitro*, CSE inhibition decreased H₂S levels and restored ferroptosis in Fer-1-treated HUCMSCs. Interestingly, we found that upregulation of the CSE/H₂S pathway induced the S-sulfhydration of Keap1, which contributed to the inhibition of ferroptosis.

Research conclusions

Regulation of the CSE/H₂S pathway in HUCMSCs contributes to the inhibition of ferroptosis and improves the effect of vascular remodelling suppression in hypoxia-induced PAH mice. Moreover, the protective effect of the CSE/H₂S pathway on ferroptosis in HUCMSCs is mediated *via* S-sulfhydrated Keap1/nuclear factor erythroid 2-related factor 2 (Nrf2) signalling. The present study may provide a novel therapeutic avenue for improving the protective capacity of transplanted MSCs in PAH.

Research perspectives

Regulation of the CSE/H₂S pathway in HUCMSCs contributes to the inhibition of ferroptosis and improves the ability of HUCMSCs to suppress vascular remodelling in mice with hypoxia-induced PAH. Moreover, the protective effect of the CSE/H₂S pathway on ferroptosis in HUCMSCs is mediated *via* S-sulfhydrated Keap1/Nrf2 signalling. The present study may provide a novel therapeutic avenue for improving the protective capacity of transplanted MSCs in PAH.

FOOTNOTES

Co-first authors: Bin Hu and Xiang-Xi Zhang.

Author contributions: Hu B and Zhang XX contributed equally to this work; Yu WC conceived the research; Hu B and Yu WC participated in the design of the study, performed the statistical analysis, and helped to draft the manuscript; Hu B, Zhang XX, Zhang T, and Yu WC performed the experiments; and all authors participated in discussing and revising the manuscript, and approving the final manuscript.

Supported by the Natural Science Foundation of Shandong Province of China, No. ZR2021QH179 and ZR2020MH014.

Institutional animal care and use committee statement: Animal procedures were performed in compliance with the Institutional Animal Care and Use Committee of Shandong Provincial Hospital Affiliated to Shandong First Medical University (No. 2022-333).

Conflict-of-interest statement: All the authors report no relevant conflicts of interest for this article.

Data sharing statement: No additional unpublished data are available.

ARRIVE guidelines statement: The authors have read the ARRIVE guidelines, and the manuscript was prepared and revised according to the ARRIVE guidelines.

Open-Access: This article is an open-access article that was selected by an in-house editor and fully peer-reviewed by external reviewers. It is distributed in accordance with the Creative Commons Attribution NonCommercial (CC BY-NC 4.0) license, which permits others to distribute, remix, adapt, build upon this work non-commercially, and license their derivative works on different terms, provided the original work is properly cited and the use is non-commercial. See: <https://creativecommons.org/licenses/by-nc/4.0/>

Country/Territory of origin: China

ORCID number: Wan-Cheng Yu 0000-0003-3850-3298.

S-Editor: Wang JJ

L-Editor: Wang TQ

P-Editor: Zhang XD

REFERENCES

- 1 Pullamsetti SS, Schermuly R, Ghofrani A, Weissmann N, Grimminger F, Seeger W. Novel and emerging therapies for pulmonary hypertension. *Am J Respir Crit Care Med* 2014; **189**: 394-400 [PMID: 24401129 DOI: 10.1164/rccm.201308-1543PP]
- 2 Malliaras K, Marbán E. Cardiac cell therapy: where we've been, where we are, and where we should be headed. *Br Med Bull* 2011; **98**: 161-185 [PMID: 21652595 DOI: 10.1093/bmb/ldr018]
- 3 Zhang Q, Wan XX, Hu XM, Zhao WJ, Ban XX, Huang YX, Yan WT, Xiong K. Targeting Programmed Cell Death to Improve Stem Cell Therapy: Implications for Treating Diabetes and Diabetes-Related Diseases. *Front Cell Dev Biol* 2021; **9**: 809656 [PMID: 34977045 DOI: 10.3389/fcell.2021.809656]
- 4 Lei G, Zhuang L, Gan B. Targeting ferroptosis as a vulnerability in cancer. *Nat Rev Cancer* 2022; **22**: 381-396 [PMID: 35338310 DOI: 10.1038/s41568-022-00459-0]
- 5 Li X, Zeng J, Liu Y, Liang M, Liu Q, Li Z, Zhao X, Chen D. Inhibitory Effect and Mechanism of Action of Quercetin and Quercetin Diels-Alder anti-Dimer on Erastin-Induced Ferroptosis in Bone Marrow-Derived Mesenchymal Stem Cells. *Antioxidants (Basel)* 2020; **9** [PMID: 32131401 DOI: 10.3390/antiox9030205]
- 6 Liu J, Ren Z, Yang L, Zhu L, Li Y, Bie C, Liu H, Ji Y, Chen D, Zhu M, Kuang W. The NSUN5-FTH1/FTL pathway mediates ferroptosis in bone marrow-derived mesenchymal stem cells. *Cell Death Discov* 2022; **8**: 99 [PMID: 35249107 DOI: 10.1038/s41420-022-00902-z]
- 7 Lan D, Qi S, Yao C, Li X, Liu H, Wang D, Wang Y. Quercetin protects rat BMSCs from oxidative stress via ferroptosis. *J Mol Endocrinol* 2022; **69**: 401-413 [PMID: 35900382 DOI: 10.1530/JME-22-0086]
- 8 Lan D, Yao C, Li X, Liu H, Wang D, Wang Y, Qi S. Tocopherol attenuates the oxidative stress of BMSCs by inhibiting ferroptosis through the PI3k/AKT/mTOR pathway. *Front Bioeng Biotechnol* 2022; **10**: 938520 [PMID: 36061427 DOI: 10.3389/fbioe.2022.938520]
- 9 Han L, Ma C, Wu Z, Xu H, Li H, Pan G. AhR-STAT3-HO-1/COX-2 signalling pathway may restrict ferroptosis and improve hMSC accumulation and efficacy in mouse liver. *Br J Pharmacol* 2023 [PMID: 37538043 DOI: 10.1111/bph.16208]
- 10 Kajarabille N, Latunde-Dada GO. Programmed Cell-Death by Ferroptosis: Antioxidants as Mitigators. *Int J Mol Sci* 2019; **20** [PMID: 31597407 DOI: 10.3390/ijms20194968]
- 11 Dodson M, Castro-Portuguez R, Zhang DD. NRF2 plays a critical role in mitigating lipid peroxidation and ferroptosis. *Redox Biol* 2019; **23**: 101107 [PMID: 30692038 DOI: 10.1016/j.redox.2019.101107]
- 12 Stein A, Bailey SM. Redox Biology of Hydrogen Sulfide: Implications for Physiology, Pathophysiology, and Pharmacology. *Redox Biol* 2013; **1**: 32-39 [PMID: 23795345 DOI: 10.1016/j.redox.2012.11.006]
- 13 Stipanuk MH. Sulfur amino acid metabolism: pathways for production and removal of homocysteine and cysteine. *Annu Rev Nutr* 2004; **24**: 539-577 [PMID: 15189131 DOI: 10.1146/annurev.nutr.24.012003.132418]
- 14 Huang F, Gao T, Wang W, Wang L, Xie Y, Tai C, Liu S, Cui Y, Wang B. Engineered basic fibroblast growth factor-overexpressing human umbilical cord-derived mesenchymal stem cells improve the proliferation and neuronal differentiation of endogenous neural stem cells and functional recovery of spinal cord injury by activating the PI3K-Akt-GSK-3 β signaling pathway. *Stem Cell Res Ther* 2021; **12**: 468 [PMID: 34419172 DOI: 10.1186/s13287-021-02537-w]
- 15 Zhang Q, Cheng X, Zhang H, Zhang T, Wang Z, Zhang W, Yu W. Dissecting molecular mechanisms underlying H₂O₂-induced apoptosis of mouse bone marrow mesenchymal stem cell: role of Mst1 inhibition. *Stem Cell Res Ther* 2020; **11**: 526 [PMID: 33298178 DOI: 10.1186/s13287-020-02041-7]
- 16 Park CM, Macinkovic I, Filipovic MR, Xian M. Use of the "tag-switch" method for the detection of protein S-sulphydration. *Methods Enzymol* 2015; **555**: 39-56 [PMID: 25747474 DOI: 10.1016/bs.mie.2014.11.033]
- 17 Yu WC, Chen HY, Yang HL, Xia P, Zou CW, Sun TW, Wang LX. rBMSC/Cav-1(F92A) Mediates Oxidative Stress in PAH Rat by

- Regulating Selw/14-3-3 η and CA1/Kininogen Signal Transduction. *Stem Cells Int* 2019; **2019**: 6768571 [PMID: 31781243 DOI: 10.1155/2019/6768571]
- 18 **Li B**, Wang C, Lu P, Ji Y, Wang X, Liu C, Lu X, Xu X. IDH1 Promotes Foam Cell Formation by Aggravating Macrophage Ferroptosis. *Biology (Basel)* 2022; **11** [PMID: 36290297 DOI: 10.3390/biology11101392]
- 19 **Pulido T**, Adzerikho I, Channick RN, Delcroix M, Galiè N, Ghofrani HA, Jansa P, Jing ZC, Le Brun FO, Mehta S, Mittelholzer CM, Perchenet L, Sastry BK, Sitbon O, Souza R, Torbicki A, Zeng X, Rubin LJ, Simonneau G; SERAPHIN Investigators. Macitentan and morbidity and mortality in pulmonary arterial hypertension. *N Engl J Med* 2013; **369**: 809-818 [PMID: 23984728 DOI: 10.1056/NEJMoa1213917]
- 20 **Arciniegas E**, Frid MG, Douglas IS, Stenmark KR. Perspectives on endothelial-to-mesenchymal transition: potential contribution to vascular remodeling in chronic pulmonary hypertension. *Am J Physiol Lung Cell Mol Physiol* 2007; **293**: L1-L8 [PMID: 17384082 DOI: 10.1152/ajplung.00378.2006]
- 21 **Zhu P**, Huang L, Ge X, Yan F, Wu R, Ao Q. Transdifferentiation of pulmonary arteriolar endothelial cells into smooth muscle-like cells regulated by myocardin involved in hypoxia-induced pulmonary vascular remodelling. *Int J Exp Pathol* 2006; **87**: 463-474 [PMID: 17222214 DOI: 10.1111/j.1365-2613.2006.00503.x]
- 22 **Piera-Velazquez S**, Jimenez SA. Molecular mechanisms of endothelial to mesenchymal cell transition (EndoMT) in experimentally induced fibrotic diseases. *Fibrogenesis Tissue Repair* 2012; **5**: S7 [PMID: 23259736 DOI: 10.1186/1755-1536-5-S1-S7]
- 23 **Yang WS**, Kim KJ, Gaschler MM, Patel M, Shchepinov MS, Stockwell BR. Peroxidation of polyunsaturated fatty acids by lipoxygenases drives ferroptosis. *Proc Natl Acad Sci U S A* 2016; **113**: E4966-E4975 [PMID: 27506793 DOI: 10.1073/pnas.1603244113]
- 24 **Battaglia AM**, Chirillo R, Aversa I, Sacco A, Costanzo F, Biamonte F. Ferroptosis and Cancer: Mitochondria Meet the "Iron Maiden" Cell Death. *Cells* 2020; **9** [PMID: 32575749 DOI: 10.3390/cells9061505]
- 25 **Park E**, Chung SW. ROS-mediated autophagy increases intracellular iron levels and ferroptosis by ferritin and transferrin receptor regulation. *Cell Death Dis* 2019; **10**: 822 [PMID: 31659150 DOI: 10.1038/s41419-019-2064-5]
- 26 **Doll S**, Freitas FP, Shah R, Aldrovandi M, da Silva MC, Ingold I, Goya Grocin A, Xavier da Silva TN, Panzilius E, Scheel CH, Mourão A, Buday K, Sato M, Wanninger J, Vignane T, Mohana V, Rehberg M, Flatley A, Schepers A, Kurz A, White D, Sauer M, Sattler M, Tate EW, Schmitz W, Schulze A, O'Donnell V, Proneth B, Popowicz GM, Pratt DA, Angeli JPF, Conrad M. FSP1 is a glutathione-independent ferroptosis suppressor. *Nature* 2019; **575**: 693-698 [PMID: 31634899 DOI: 10.1038/s41586-019-1707-0]
- 27 **Fujii J**, Homma T, Kobayashi S. Ferroptosis caused by cysteine insufficiency and oxidative insult. *Free Radic Res* 2020; **54**: 969-980 [PMID: 31505959 DOI: 10.1080/10715762.2019.1666983]
- 28 **Lu SC**. Glutathione synthesis. *Biochim Biophys Acta* 2013; **1830**: 3143-3153 [PMID: 22995213 DOI: 10.1016/j.bbagen.2012.09.008]
- 29 **Dixon SJ**, Lemberg KM, Lamprecht MR, Skouta R, Zaitsev EM, Gleason CE, Patel DN, Bauer AJ, Cantley AM, Yang WS, Morrison B 3rd, Stockwell BR. Ferroptosis: an iron-dependent form of nonapoptotic cell death. *Cell* 2012; **149**: 1060-1072 [PMID: 22632970 DOI: 10.1016/j.cell.2012.03.042]
- 30 **Yan B**, Xie D, Wu Y, Wang S, Zhang X, Zhao T, Liu L, Ma P, Li G, Yang Y, Zhao Y, Zheng T, Geng R, Li B, Zheng Q. Ferroptosis is involved in PGPS-induced otitis media in C57BL/6 mice. *Cell Death Discov* 2022; **8**: 217 [PMID: 35449198 DOI: 10.1038/s41420-022-01025-1]
- 31 **Shou Y**, Yang L, Yang Y, Xu J. Inhibition of keratinocyte ferroptosis suppresses psoriatic inflammation. *Cell Death Dis* 2021; **12**: 1009 [PMID: 34707088 DOI: 10.1038/s41419-021-04284-5]
- 32 **Kimura H**. Hydrogen sulfide: its production, release and functions. *Amino Acids* 2011; **41**: 113-121 [PMID: 20191298 DOI: 10.1007/s00726-010-0510-x]
- 33 **Kimura Y**, Goto Y, Kimura H. Hydrogen sulfide increases glutathione production and suppresses oxidative stress in mitochondria. *Antioxid Redox Signal* 2010; **12**: 1-13 [PMID: 19852698 DOI: 10.1089/ars.2008.2282]
- 34 **Wang Q**, Wang XL, Liu HR, Rose P, Zhu YZ. Protective effects of cysteine analogues on acute myocardial ischemia: novel modulators of endogenous H(2)S production. *Antioxid Redox Signal* 2010; **12**: 1155-1165 [PMID: 19842912 DOI: 10.1089/ars.2009.2947]
- 35 **Kimura Y**, Kimura H. Hydrogen sulfide protects neurons from oxidative stress. *FASEB J* 2004; **18**: 1165-1167 [PMID: 15155563 DOI: 10.1096/fj.04-1815fje]
- 36 **Sun X**, Ou Z, Chen R, Niu X, Chen D, Kang R, Tang D. Activation of the p62-Keap1-NRF2 pathway protects against ferroptosis in hepatocellular carcinoma cells. *Hepatology* 2016; **63**: 173-184 [PMID: 26403645 DOI: 10.1002/hep.28251]
- 37 **Shin D**, Kim EH, Lee J, Roh JL. Nrf2 inhibition reverses resistance to GPX4 inhibitor-induced ferroptosis in head and neck cancer. *Free Radic Biol Med* 2018; **129**: 454-462 [PMID: 30339884 DOI: 10.1016/j.freeradbiomed.2018.10.426]
- 38 **Fan Z**, Wirth AK, Chen D, Wruck CJ, Rauh M, Buchfelder M, Savaskan N. Nrf2-Keap1 pathway promotes cell proliferation and diminishes ferroptosis. *Oncogenesis* 2017; **6**: e371 [PMID: 28805788 DOI: 10.1038/oncsis.2017.65]
- 39 **Abed DA**, Goldstein M, Albanyan H, Jin H, Hu L. Discovery of direct inhibitors of Keap1-Nrf2 protein-protein interaction as potential therapeutic and preventive agents. *Acta Pharm Sin B* 2015; **5**: 285-299 [PMID: 26579458 DOI: 10.1016/j.apsb.2015.05.008]
- 40 **Mustafa AK**, Gadalla MM, Sen N, Kim S, Mu W, Gazi SK, Barrow RK, Yang G, Wang R, Snyder SH. H2S signals through protein S-sulfhydration. *Sci Signal* 2009; **2**: ra72 [PMID: 19903941 DOI: 10.1126/scisignal.2000464]
- 41 **Xie L**, Gu Y, Wen M, Zhao S, Wang W, Ma Y, Meng G, Han Y, Wang Y, Liu G, Moore PK, Wang X, Wang H, Zhang Z, Yu Y, Ferro A, Huang Z, Ji Y. Hydrogen Sulfide Induces Keap1 S-sulfhydration and Suppresses Diabetes-Accelerated Atherosclerosis via Nrf2 Activation. *Diabetes* 2016; **65**: 3171-3184 [PMID: 27335232 DOI: 10.2337/db16-0020]



Published by **Baishideng Publishing Group Inc**
7041 Koll Center Parkway, Suite 160, Pleasanton, CA 94566, USA
Telephone: +1-925-3991568
E-mail: bpgoffice@wjgnet.com
Help Desk: <https://www.f6publishing.com/helpdesk>
<https://www.wjgnet.com>

